Optimum Surface Plasmon Excitation and Propagation on Conductive Two-Dimensional Materials and Thin Films

Feng Liang, Alexander B. Yakovlev, *Senior Member, IEEE*, and George W. Hanson, *Fellow, IEEE*

***Abstract*—The surface conductivity of two-dimensional (2-D) materials and thin conductive films is considered for surface plasmon (SP) excitation and propagation. It is shown that an ideal surface conductivity exists to maximize the SP field at a given position, based on a tradeoff relating to propagation loss and near-field excitation amplitude associated with the local density of photonic states. Dispersionless and Drude dispersion models are considered, as well as the effect of interband transitions. Simple formulas are presented to obtain a maximal SP field at a given distance from a canonical source. Examples are shown for graphene and thin metal films, and a discussion of the competition between propagation loss and SP excitation is provided.**

***Index Terms*—Graphene, surface plasmon (SP), thin films.**

I. Introduction

BECAUSE of their ability to confine light in subwavelength spaces, surface plasmons (SPs) are of considerable importance in a variety of areas, including optical sensors, optical antennas, solar cells, near-field communications, and data storage [1]. SPs can be confined to a planar-like surface and propagate along the surface, and are sometimes called surface plasmon polaritons (SPPs), or they can be nonpropagating and confined to the surface of metallic particles or curved metal objects, in which case they are called localized surface plasmons (LSPs) [2] or particle plasmons. The main attributes of both SPPs and LSPs are high electric field amplitudes and subwavelength energy confinement. Although SPPs and LSPs have many overlapping applications, uses of SPPs often involve their propagation aspects for communications or sensing [3]–[6], and many LSP applications center on their small size and stationary nature, such as creating localized hot-spots for biological/medical imaging and cancer treatment [7], [8]. Planar structures having propagating SPs are larger than typical LSP structures, but are generally easier to fabricate and one does not need to precisely position nanoparticles as is often required for LSP applications.

Surface plasmons on two-dimensional (2-D) planar materials such as graphene and $\mathrm{MoS_2}$, and on very thin three-dimensional (3-D) materials such as thin metal layers, doped semiconductor films, and 2-D electron gasses are of considerable interest [9]–[15]. In all cases, the surface can be modeled by a surface conductivity σ (S), and which can be controlled by chemical doping and, for some materials like graphene and even thin metals, can be controlled by an external dc electric or magnetic field bias [16], [17]. Frequency dispersion typically dictates a desirable frequency range for strong SP propagation. Moreover, although it is beyond the scope of the present work, one can engineer artificial surfaces to achieve desirable characteristics (often analyzed by 2-D homogenization) [18]–[20].

In general, σ is complex valued, with the real part being associated with loss (absorption) and the imaginary part being associated with reactive energy storage. For many materials of interest, there is a Drude component and an interband component; $\mathrm{Im}(\sigma) < 0$ for the Drude component is inductive due to the kinetic energy of charge carriers, whereas for the interband component $\mathrm{Im}(\sigma) > 0$ is related to capacitance associated with band transitions. Loss is associated with $\mathrm{Re}(\sigma)$ due to electronic collisions with phonons, impurities, lattice imperfections, and band transitions.

Given that the value of σ can be controlled by a range of geometrical and electrical parameters, an important question arises as to the optimal surface characteristics for SP excitation and propagation. Obviously, we generally want a low-loss structure, and so we will assume that $\mathrm{Im}(\sigma) \gg \mathrm{Re}(\sigma)$ to have low surface plasmon absorption, and also that the permittivity of the material surrounding the surface has low dielectric loss. In this work, we consider the optimum value of the surface conductivity of a 2-D surface and thin film for strong SP excitation and propagation. We consider several different models of increasing complexity, including dispersionless and Drude dispersion models, as well as the effect of interband transitions, to achieve desirable SP characteristics.

II. Surface Plasmon and Total Fields on a 2-D Surface

Consider an infinite 2-D material sheet with surface conductivity $\sigma = \sigma' - j\sigma''$ immersed in a multilayered environment as depicted in Fig. 1. In each region, the permittivity may

Manuscript received September 12, 2014; revised December 14, 2014; accepted January 18, 2015. Date of publication January 22, 2015; date of current version April 03, 2015. This work was supported in part by the National Natural Science Foundation of China under Grant 61204041 and Grant 61331007, in part by the China Postdoctoral Science Foundation funded project under Grant 2014M552335, in part by the Fundamental Research Funds for the Central Universities of China under Grant ZYGX2013J049, and in part by the China Scholarship Council.

F. Liang is with the School of Physical Electronics, University of Electronic Science and Technology of China, Chengdu 610054, China (e-mail: fengliang@uestc.edu.cn).

A. B. Yakovlev is with the Department of Electrical Engineering, University of Mississippi, Oxford, MI 38677 USA (e-mail: yakovlev@olemiss.edu).

G. W. Hanson is with the Department of Electrical Engineering, University of Wisconsin–Milwaukee, Milwaukee, WI 53211 USA (e-mail: george@uwm.edu).

Color versions of one or more of the figures in this paper are available online at http://ieeexplore.ieee.org.

Digital Object Identifier 10.1109/TAP.2015.2395440

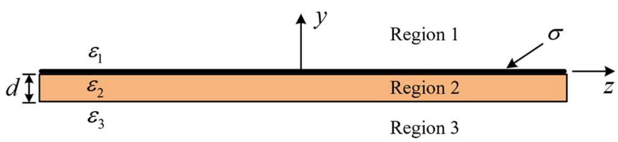

Fig. 1. Cross-sectional view of 2-D material sheet with surface conductivity σ immersed in a multilayer environment.

be complex-valued, $\varepsilon = \varepsilon_0\varepsilon_r = \varepsilon_0(\varepsilon_r' - j\varepsilon_r'')$, where the suppressed time variation is $e^{j\omega t}$. The electric field in the nth region is [21]

$$\mathbf{E}^{(n)}(\mathbf{r},\omega) = \frac{1}{j\omega\varepsilon_n}\int \underline{\mathbf{G}}^{(n)}(\mathbf{r},\mathbf{r}',\omega)\cdot\mathbf{J}(\mathbf{r}')\,d\Omega' \tag{1}$$

where Ω is the support of the current and where the dyadic Green function is

$$\nabla\times\nabla\times\underline{\mathbf{G}}^{(n)}(\mathbf{r},\mathbf{r}',\omega) - k_n^2\underline{\mathbf{G}}^{(n)}(\mathbf{r},\mathbf{r}',\omega) = k_n^2\underline{\underline{\mathbf{I}}}\,\delta(\mathbf{r}-\mathbf{r}') \tag{2}$$

and where $k_n = \omega\sqrt{\varepsilon_n\mu_n}$ is the wavenumber in region n (we consider the special case where the field observation point and the current reside in the same layer, and all materials are nonmagnetic). Assuming that the sheet is excited by a vertical Hertzian dipole current at distance y_0 above the surface, $\mathbf{J}(\mathbf{r}) = \hat{\mathbf{y}}\delta(x)\delta(y-y_0)\delta(z)$, then only TM modes can be excited (we assume $\sigma'' > 0$ as discussed below) and the electric field in Region 1 is [11], [21]

$$\begin{aligned}\mathbf{E}^{(1)}(\mathbf{r}) = \frac{1}{8\pi j\omega\varepsilon_1}&\left[\left(\hat{\mathbf{x}}\frac{x}{\rho} + \hat{\mathbf{z}}\frac{z}{\rho}\right)\right.\\ &\int_{-\infty}^{\infty} -k_\rho^2(e^{-p_1|y-y_0|} + R_N e^{-p_1(y+y_0)})H_0^{(2)\prime}(k_\rho\rho)dk_\rho\\ &\left.+\,\hat{\mathbf{y}}\int_{-\infty}^{\infty}\frac{k_\rho^3}{p_1}(e^{-p_1|y-y_0|} + R_N e^{-p_1(y+y_0)})H_0^{(2)}(k_\rho\rho)dk_\rho\right]\end{aligned} \tag{3}$$

where k_ρ is the radial wavenumber, $\rho = \sqrt{x^2+z^2}$, $p_n = \sqrt{k_\rho^2 - k_n^2}$, and

$$R_N = \frac{N^E}{Z^E} = \frac{A^-\cosh(p_2 d) + B^-\sinh(p_2 d)}{A^+\cosh(p_2 d) + B^+\sinh(p_2 d)} \tag{4}$$

with

$$\begin{aligned}A^\pm &= \varepsilon_2\left(\frac{p_1 p_3\sigma}{j\omega} + p_1\varepsilon_3 \pm \varepsilon_1 p_3\right)\\ B^\pm &= p_2\left(\frac{p_1 p_3\varepsilon_2^2}{p_2^2} \pm \varepsilon_1\varepsilon_3 + \frac{p_1\varepsilon_3\sigma}{j\omega}\right).\end{aligned}$$

The first terms in each of the Sommerfeld integrals in (3) represent the primary field due to the source without the 2-D material sheet (and can be evaluated in closed form), and the second terms in each integral represent the surface and dielectric contributions. These can be decomposed as an SP term (analytically evaluated by the residue of the Sommerfeld integral), and a branch cut contribution representing the radiation spectra, which can be numerically computed along the integration path depicted in [12]. That is, $E = E_{\mathrm{h}} + E_{\mathrm{residue}} + E_{\mathrm{bc}}$. Specifically, the electric field in Region 1 due to the surface plasmon is

$$\begin{aligned}\mathbf{E}^{(1)}_{\mathrm{residue}}(y,\rho) = \frac{(k_\rho^{\mathrm{SP}})^2 R_N'}{4\omega\varepsilon_1}e^{-\sqrt{(k_\rho^{\mathrm{SP}})^2-k_1^2}(y+y_0)}&\left[\left(\hat{\mathbf{x}}\frac{x}{\rho} + \hat{\mathbf{z}}\frac{z}{\rho}\right)\right.\\ \times H_0^{(2)\prime}(k_\rho^{\mathrm{SP}}\rho) - \hat{\mathbf{y}}&\left.\frac{k_\rho^{\mathrm{SP}}H_0^{(2)}(k_\rho^{\mathrm{SP}}\rho)}{\sqrt{(k_\rho^{\mathrm{SP}})^2-k_1^2}}\right]\end{aligned} \tag{5}$$

where $R_N' = N^E/(\partial Z^E/\partial k_\rho)$ and $H_0^{(2)\prime}(\alpha) = \partial H_0^{(2)}(\alpha)/\partial\alpha$, and where all quantities are evaluated at the SP wavenumber k_ρ^{SP} obtained from the dispersion equation discussed in Section III. This SP field is the desired one to maximize. For simplicity, we consider the vertical component of the electric field as follows:

$$\begin{aligned}E^{(1)}_{y,\mathrm{residue}}(y,\rho) &= \frac{1}{j\omega\varepsilon_1}G^{(1)}_{yy,\mathrm{residue}}(y,\rho)\\ &= -\frac{(k_\rho^{\mathrm{SP}})^3 R_N'}{4\omega\varepsilon_1}\frac{e^{-\sqrt{(k_\rho^{\mathrm{SP}})^2-k_1^2}(y+y_0)}}{\sqrt{(k_\rho^{\mathrm{SP}})^2-k_1^2}}\\ &\quad\times H_0^{(2)}(k_\rho^{\mathrm{SP}}\rho).\end{aligned} \tag{6}$$

The photonic local density of states (LDOS) [22] projected along the dipole orientation associated with the SP field is

$$\begin{aligned}\rho_{yy}^{\mathrm{SP}}(y_0,k_\rho^{\mathrm{SP}}) &= \frac{6}{\pi\omega}\mathrm{Im}\left(G^{(1)}_{yy,\mathrm{residue}}(\mathbf{r},\mathbf{r},\omega)\right)\\ &= \frac{6}{\pi\omega}\mathrm{Re}\left((k_\rho^{\mathrm{SP}})^3 R_N'\frac{e^{-\sqrt{(k_\rho^{\mathrm{SP}})^2-k_1^2}2y_0}}{4\sqrt{(k_\rho^{\mathrm{SP}})^2-k_1^2}}\right.\\ &\quad\left.\times\, H_0^{(2)}(k_\rho^{\mathrm{SP}}\rho\to 0)\right)\end{aligned} \tag{7}$$

since the source is located at $(0,y_0,0)$. Using $H_0^{(2)}(z\to 0) = 1 - j\frac{2}{\pi}\left[\ln\left(\frac{z\to 0}{2}\right) + \cdots\right]$ where the remaining terms are finite at $z = 0$, in the lossless case, the coefficient preceding the Hankel function is real-valued, and the LDOS is finite. However, it is well known that in a lossy environment the LDOS diverges due to a breakdown of the dipole approximation. Various methods of regularizing the Green function for the lossy case have been proposed, such as averaging over a small cavity volume containing the emitter, thereby regularizing the divergent term (i.e., integrating over the exclusion volume in the depolarizing dyadic contribution to the field [23]). For our purposes, it is enough to know that

$$\rho_{yy}^{\mathrm{SP}}(y_0,k_\rho^{\mathrm{SP}}) \propto \frac{6}{\pi\omega}\mathrm{Re}\left((k_\rho^{\mathrm{SP}})^3 R_N'\frac{e^{-\sqrt{(k_\rho^{\mathrm{SP}})^2-k_1^2}2y_0}}{4\sqrt{(k_\rho^{\mathrm{SP}})^2-k_1^2}}\right) \tag{8}$$

where the proportionality factor is unity for lossless media.

Although the LDOS is often associated with the decay rate of a quantum emitter, it more generally relates to field concentration, with higher LDOS associated with strong field values [22].

Although the LDOS is defined for $\mathbf{r} = \mathbf{r}'$, in the following, we allow the vertical observation point y to be different than the vertical source point y_0 [e.g., replacing $2y_0$ with $y + y_0$ in (8)], and refer to this as a generalized LDOS.[1] The utility of this is that, although the LDOS is real-valued and the residue field is generally complex valued, it allows interpretation of the residue field as the product of a (generalized) LDOS-related factor and the Hankel function lateral propagation factor. If we have $y = y_0$ and lossless media then the residue field is precisely the product of the LDOS, the Hankel function propagation factor, and a constant $(\pi/24\varepsilon_1)$. Furthermore, for the lossless case lateral propagation loss is not an issue, and maximizing the SP field is achieved by simply maximizing the generalized LDOS. For the low-loss cases considered here, the identification of the Hankel function prefactor as a LDOS retains considerable merit.

It is also worth noting that for a lossless environment the power radiated by the dipole can be expressed as [24]

$$P_r = \frac{|\mathbf{J}|^2 \pi}{12\varepsilon} \rho_{yy} \tag{9}$$

and so maximizing overall power radiated into surface waves in a lossless environment is equivalent to maximizing the LDOS associated with surface waves. However, this does not necessarily maximize the SP field amplitude at a general point $y \neq y_0$, for that, one must maximize the generalized LDOS.

In summary, the SP field (6) can be interpreted as the product of three terms, two of which are associated with the LDOS (an amplitude term involving R'_N and a vertical decay term that governs source coupling to the exponential tail of the SP mode), and a lateral propagation factor given by the Hankel function. The interplay among these three terms leads to the existence of an optimal surface conductivity.

III. SP Modal Characteristics

The dispersion equation for the surface plasmon is obtained from $Z^E = 0$ in (4). For the general case this cannot be solved in closed form, but for the case of a homogeneous background, i.e., $\varepsilon_1 = \varepsilon_2 = \varepsilon_3 = \varepsilon$, (4) can be simplified to $R_N = \sigma p/(2j\omega\varepsilon + \sigma p)$ and the dispersion equation can be solved to yield

$$k_\rho^{\mathrm{SP}} = k\sqrt{1 - \left(\frac{2}{\sigma\eta}\right)^2} \tag{10}$$

which is the (sole) TM surface plasmon wavenumber for a 2-D surface in a homogeneous background, $\eta = \sqrt{\varepsilon/\mu}$.

[1]For LDOS applications to determine the natural decay rate of a quantum emitter, we must have $y = y_0$ since the back-reaction of the environment on the emitter, associated with the self-consistent field, must be evaluated at the location of the emitter. In the case of a classical dipole source considered here, this back-reaction has no effect as the dipole is a constant-current source, and so we can generalize the LDOS concept to allow for different source and observation vertical locations. Alternatively, we could define the vertical displacement $\Delta y = y - y_0$ and lateral displacement $\Delta\rho = \rho - \rho_0 = \rho$ and consider that the residue field is (exactly for lossless media and approximately for low-loss media) the LDOS multiplied by lateral and vertical propagation factors $H_0^{(2)}(k_\rho^{\mathrm{SP}}\Delta\rho)$ and $e^{-\sqrt{(k_\rho^{\mathrm{SP}})^2 - k_1^2}\Delta y}$ that account for displacement from the source.

Let $k = k_0\sqrt{\varepsilon_r' - j\varepsilon_r''}$, $\eta = \eta_0/\sqrt{\varepsilon_r' - j\varepsilon_r''}$, where k_0 and η_0 are the vacuum values, and assume $\sigma'' > 0$ (to have an inductive surface, in which case only TM plasmons can propagate [10], [11]), $\sigma'' \gg \sigma'$ to have low surface plasmon loss and $\varepsilon_r'' \ll \varepsilon_r'$ to have low dielectric loss. Then, from (10),

$$k_\rho^{\mathrm{SP}}/k_0 \approx \frac{2}{\sigma''\eta_0}\left(\varepsilon_r' - j\left(\varepsilon_r'' + \frac{\varepsilon_r'\sigma'}{\sigma''}\right)\right). \tag{11}$$

The real-part of k_ρ^{SP} is related to the phase velocity of the surface plasmon, $v_p = \omega/\mathrm{Re}(k_\rho^{\mathrm{SP}})$ [the ratio $\mathrm{Re}(k_\rho^{\mathrm{SP}}/k_0)$ defines the slow-wave factor], and the imaginary part of k_ρ^{SP} is associated with attenuation of the surface plasmon along the propagation direction ρ.

The propagation constant along the vertical direction can be written as $p = \sqrt{k_\rho^2 - k^2} = 2jk/(\sigma\eta)$ such that, from e^{-py}, a vertical field confinement factor $(1/e)$ can be defined as

$$\zeta/\lambda_0 = \frac{1}{\mathrm{Re}(p)\lambda_0} \approx \frac{\eta_0\sigma''}{4\pi\varepsilon_r'} \tag{12}$$

where λ_0 is the wavelength in free space. For good confinement, we need $\zeta/\lambda_0 \ll 1$. It is obvious that small σ'' leads to a large slow-wave factor and tight field confinement, but also to large propagation loss.

IV. Optimal Surface Characteristics for Maximum SP Field Amplitude

In the context of this work, we assume that surface plasmons have four desirable characteristics: the SP mode should 1) be slow $[\mathrm{Re}(k_\rho^{\mathrm{SP}})/k_0 \gg 1]$ and therefore nonradiative; 2) have tight energy confinement to the surface; 3) have low propagation loss; and 4) have a strong excitation amplitude. The first three criteria are solely based on the natural modal SP wavenumber (i.e., the mode of the infinite material surface and dielectric environment), whereas the fourth criteria is affected by both propagation associated with the modal wavenumber and with the generalized LDOS. Moreover, the first two criteria contradict the third one (and the fourth criteria is related in a nontrivial manner to the first three criteria). Maximizing the SP field can be seen to be a balance between maximizing the LDOS seen by the source, and loss associated with the lateral propagation factor.

Using the large-argument approximation of the Hankel function, (6) can be simplified to

$$|E_{y,\mathrm{residue}}| \approx C\left|\frac{(k_\rho^{\mathrm{SP}})^{\frac{3}{2}}}{\sigma} e^{-\frac{2k_0\varepsilon_r'(y+y_0)}{\eta_0\sigma''}}\right| \left|e^{\mathrm{Im}(k_\rho^{\mathrm{SP}})\rho}\right| \tag{13}$$

where C is a coefficient independent of σ. The first term $[(k_\rho^{\mathrm{SP}})^{\frac{3}{2}}/\sigma]$ comes from the amplitude factor R'_N, and the exponential term $e^{\mathrm{Im}(k_\rho^{\mathrm{SP}})\rho}$ arises from the Hankel function, the propagation factor of the surface plasmon. As σ'' decreases the first term on the right-hand side of (13) increases (consistent with the first two criteria). However, the vertical decay and lateral propagation factor terms will decrease sharply for sufficiently small σ'', placing a limit of how small σ'' can be, consistent with the third criteria concerning propagation loss. By setting $\partial\left|E_{y,\mathrm{residue}}\right|/\partial\sigma''=0$ in (13), the optimal σ'' for the maximum surface plasmon amplitude can be obtained. In the following, we consider several different material models. The appendix presents a different optimization based on modal properties (but ignores excitation).

A. Dispersionless Model

In this section, we consider a generic 2-D material and the effect of σ (particularly σ'') on the excitation and propagation characteristics of surface plasmons. We assume a dispersionless model to clarify the role of various parameters on SP excitation and propagation, and in the next section, we consider Drude dispersive models.

For dispersionless materials, σ is independent of frequency, and σ'' and σ' are also assumed independent on each other (of course, the Kramers–Kronig relations link these two quantities for a realistic causal material). By setting $\partial|E_{y,\mathrm{residue}}|/\partial\sigma''=0$ in (13), we obtain

$$\sigma''_{\mathrm{opt}}\approx\frac{2k_0(\varepsilon''_r\rho+\varepsilon'_r\tilde{y})+2\sqrt{k_0^2(\varepsilon''_r\rho+\varepsilon'_r\tilde{y})^2+10k_0\eta_0\varepsilon'_r\sigma'\rho}}{5\eta_0}\tag{14}$$

where $\tilde{y}=y+y_0$.

Equation (14) provides the optimal value of σ'' to maximize the field at the observation point (for a given fixed value of σ'), and results in a certain amount of propagation loss—it is interesting to point out that because of the competing factors of vertical mode confinement, propagation loss, and excitation amplitude/LDOS, altering σ'' to, say, reduce field confinement and decrease the modal propagation loss below the value associated with σ''_{opt} actually decreases the amplitude of the electric field at the observation point. This is partly due to the vertical decay factor in the LDOS, but even for $y=y_0=0$ there is competition between small σ'' increasing the R'_N term in the LDOS and lateral propagation loss.

In all of the following results, we assume the dipole source is located on the surface ($y_0=0$) and the observation point at $y=\lambda_0/100$. We first consider the case of a thin conductive sheet in a homogeneous environment with $\varepsilon'_r=1$ and $\varepsilon''_r=10^{-3}$.

Fig. 2 shows the normalized phase velocity, confinement factor, and power attenuation of the surface plasmon along the propagation (ρ) direction as a function of σ''. As σ'' decreases for a fixed $\sigma'=10^{-6}$ S, the phase velocity is at first constant and then decreases quickly, while the power attenuation is at first constant and then increases. Mode confinement becomes tighter as σ'' decreases. The level at which the attenuation curve settles for large σ'' depends on ε''_r, with lower ε''_r leading to lower attenuation (the effect of ϵ'' on phase velocity and mode confinement is negligible). The knee of the curve where attenuation becomes constant depends on ε'_r and σ'. It can be seen that for small lateral distance ρ (close to the source), conditions for a maximal SP field are such that modal attenuation is relatively large, and the wave is slow and has good confinement. To achieve a maximal SP field for a fixed vertical position y, as the lateral observation point ρ moves further away from the source attenuation needs to be reduced—here, via a larger value of σ'' that results in a less well confined mode. However, while very large values of σ'' minimize the lateral attenuation as shown in Fig. 2, if the value of σ'' is greater than that specified by (14) the SP field amplitude at the observation point (ρ,y) will not be maximal.

The normalized electric fields for $\rho=\lambda_0$ are shown in Fig. 3 where E_{residue}, E_{bc}, E_{total}, and E_h are the y components of the residue (SP) field, branch cut (continuous spectrum) field, total field, and the direct source-excited field without the 2-D material sheet, respectively ($E_{\mathrm{total}}=E_h+E_{\mathrm{residue}}+E_{\mathrm{bc}}$). From Fig. 3, one can observe that when σ'' decreases from 1 to 10^{-5} S, the total electric field will be dominated by different terms. For large σ'' value, i.e., $\sigma''>10^{-1}$ S, the branch cut field is quite close to the direct source-excited field, and both of them equally contribute to the total field, while the residue field is relatively small. For medium σ'', i.e., $\sigma''\in[8\times10^{-5},10^{-2}]$ S, a strong residue field occurs, which dominates the total field. For small σ'', i.e., $\sigma''\in(0,6\times10^{-5})$ S, the residue field decreases rapidly, and the direct source-excited field dominates the total

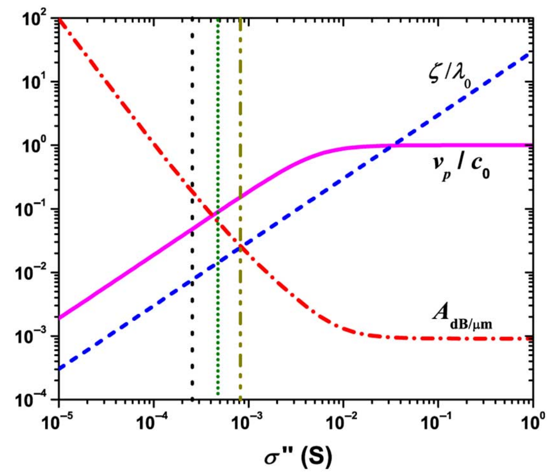

Fig. 2. Normalized phase velocity v_p/c_0 (c_0 is the speed of light in vacuum), field confinement factor ζ/λ_0, and power attenuation $A_{\mathrm{dB}/\mu\mathrm{m}}$ versus σ'', for a dispersionless model; $\sigma'=10^{-6}$ S, $f=10$ THz. The dot, short dot, and dash-dot-dot vertical lines represent the optimal σ'' from (14) for $\rho=\lambda_0$, $\rho=5\lambda_0$, and $\rho=15\lambda_0$, respectively.

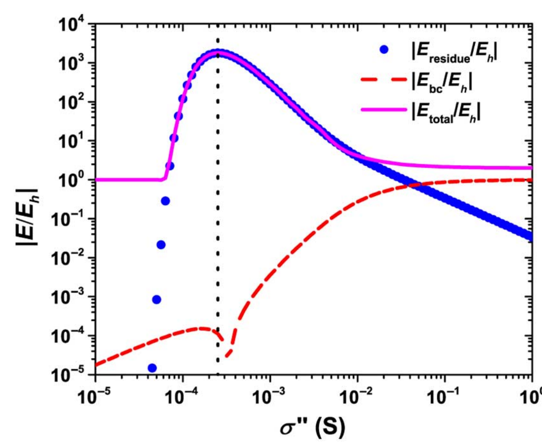

Fig. 3. Normalized electric fields versus σ'' for a dispersionless model. The vertical line represents the optimal σ'' from (14). $\sigma'=10^{-6}$ S, $f=10$ THz, $\rho=\lambda_0$.

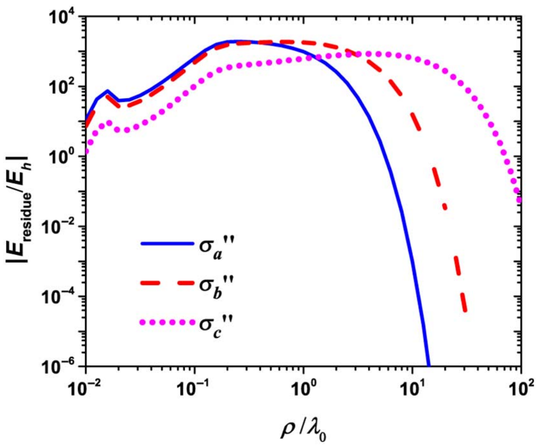

Fig. 4. Normalized surface plasmon electric field versus normalized ρ for $f = 10$ THz, and $\sigma' = 10^{-6}$ S for three different σ'' values: $\sigma_a'' = 1.52 \times 10^{-4}$ S, optimal for $\rho = 0.1\lambda_0$, $\sigma_b'' = 2.52 \times 10^{-4}$ S, optimal for $\rho = \lambda_0$, and $\sigma_c'' = 6.67 \times 10^{-4}$ S, optimal for $\rho = 10\lambda_0$.

field (since we assume $\sigma' \ll \sigma''$, as σ'' decreases toward zero the 2-D material essentially vanishes).

From Fig. 3, it is obvious that the value from (14), $\sigma''_{\mathrm{opt}} = 0.00025$ S, maximizes the electric field. The associated attenuation is $A \approx 0.19$ dB/μm and $\zeta/\lambda_0 \approx 0.0076$. As shown in Fig. 2, as the observation point (ρ) increases, σ''_{opt} increases, reducing attenuation. However, the observation point would need to be approximately $\rho \approx 600\lambda_0$ for σ''_{opt} to reach the point of minimum modal attenuation ($\sigma'' \approx 0.01$ S).

Moreover, the effect of the source and observation point positions above the surface is important. As $\tilde{y}$ in (14) increases, the value of σ''_{opt} increases, decreasing field confinement. Clearly, this is related to the vertical position of the source and/or the observation point above the graphene—for a given position the field maximum is associated with the value of σ'' at which the field couples strongly to the exponential tail of the SP mode.

Given the position dependance of (14), the SP field versus ρ for different σ'' values is of interest. Fig. 4 shows the SP field for σ'' optimized at three different radial distances: $\rho = 0.1\lambda_0$ ($\sigma_a'' = 1.52 \times 10^{-4}$ S), $\rho = \lambda_0$ ($\sigma_b'' = 2.52 \times 10^{-4}$ S), and $\rho = 10\lambda_0$ ($\sigma_c'' = 6.67 \times 10^{-4}$ S). The magnitude of the field is more sensitive to ρ for σ'' optimized for smaller ρ, whereas the field is more uniform when optimized for a larger ρ.

B. Drude Dispersion Model

The dispersionless model is not realistic except as an approximation over a fairly narrow frequency range. In this section, we consider a material with Drude dispersion having 2-D conductivity of the form

$$\sigma(\omega) = \frac{\sigma_0}{1 + j\omega\tau} \tag{15}$$

where τ is the relaxation time ($\nu = 1/\tau$ is the relaxation frequency) and σ_0 is the static 2-D conductivity (S). For thin films, $\sigma_0 = \sigma_{3\text{-D}} t$, where $\sigma_{3\text{-D}}$ is the usual 3-D conductivity, $\sigma_{3\text{-D}} = e^2 n\tau/m$, where e is charge, n is the carrier number density, m is the charge mass, and t is the film thickness. For

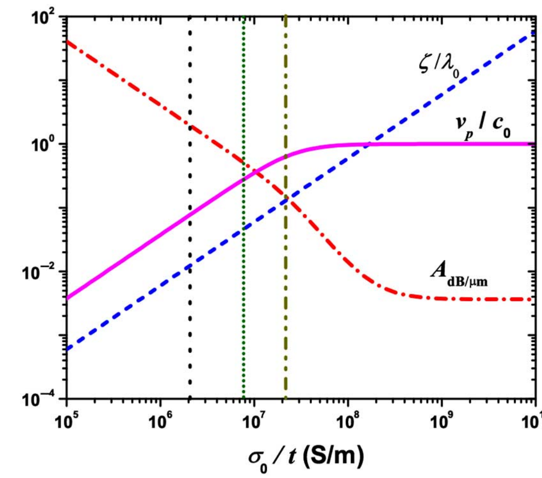

Fig. 5. Normalized phase velocity v_p/c_0, field confinement factor ζ/λ_0, and power attenuation $A_{\mathrm{dB}/\mu\mathrm{m}}$ versus σ_0 for general Drude dispersion model with $t = 10$ nm, $\tau = 0.2$ ps, $f = 40$ THz. The dot, short dot, and dash-dot-dot vertical lines represent the optimal σ_0 from (16) for $\rho = \lambda_0$, $\rho = 5\lambda_0$, and $\rho = 15\lambda_0$, respectively.

$\omega\tau \ll 1$, $\sigma' \gg \sigma''$ and the sheet is relatively lossy, and for $\omega\tau > 1$, $\sigma'' > \sigma'$ and the sheet has relatively low loss. Although $\sigma''/\sigma' = \omega\tau$ increases linearly as frequency increases, both σ' and σ'' decrease with increasing frequency above $\omega\tau = 1$, and so to have $\sigma'' \gg \sigma'$ as considered in the analysis, and to obtain a sufficiently large value of σ'', one needs to have $\omega\tau > 1$ but not $\omega\tau \gg 1$.

The Drude model is very applicable to 2-D surfaces and thin conductive films (below the range of interband transitions, otherwise augmented by interband transitions as described in the next section), e.g., Drude materials include graphene [12], metal films [25], boron-doped diamond films [26], Sb-doped SnO_2 thin films [27], and Al-doped ZnO thin films [28], to name just a few. In general, any sufficiently conductive material (i.e., with a sufficient number density of free electrons) will be plasma-like and will often be well-approximated by the Drude model.

Differing from the dispersionless model, σ' and σ'' are related to each other in the Drude model, i.e., $\sigma' = \sigma''/(\omega\tau)$, and where it can be noted that the Drude model satisfies causality and obeys the Kramers–Kronig relations. Setting $\partial |E_{y,\mathrm{residue}}| / \partial\sigma_0 = 0$, we obtain

$$\sigma_{0,\mathrm{opt}} \approx \frac{4k_0\varepsilon_r'(1+(\omega\tau)^2)}{5\eta_0\omega\tau}\left[\left(\frac{\varepsilon_r''}{\varepsilon_r'} + \frac{1}{\omega\tau}\right)\rho + \tilde{y}\right]. \tag{16}$$

In general, one can adjust σ_0 (e.g., by adjusting the number density of free carriers n) to obtain a maximum SP field. In the following examples, we assume film thickness $t = 10$ nm, relaxation time $\tau = 0.2$ ps, and frequency 40 THz.

Fig. 5 shows the normalized phase velocity, confinement factor, and power attenuation of the surface plasmon along the propagation (ρ) direction as a function of σ_0, and Fig. 6 shows the corresponding electric field as a function of σ_0. The optimal value of σ_0 from (16) is also shown.

Fig. 7 shows the optimal σ_0 predicted by (16), and the value determined (extracted) from the numerical field curves for a

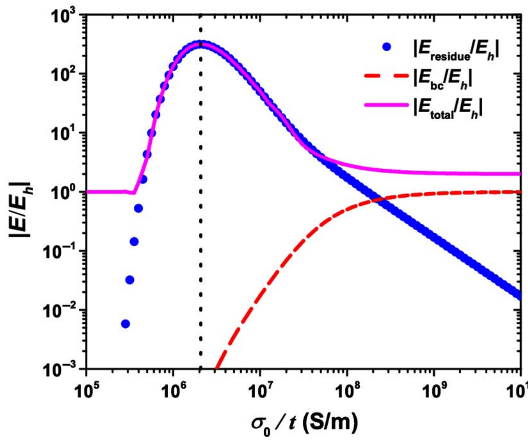

Fig. 6. Normalized electric fields versus σ_0 for general Drude dispersion model with $t = 10$ nm, $\tau = 0.2$ ps, $f = 40$ THz, $\rho = \lambda_0$. The vertical line represents the optimal σ_0 from (16).

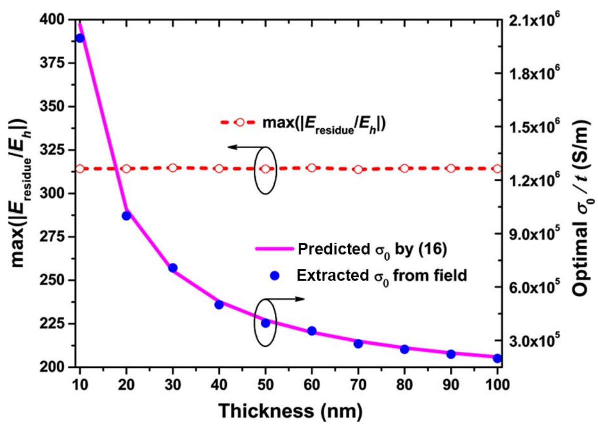

Fig. 7. Maximum normalized electric fields, optimal σ_0 versus film thickness predicted by (16) and extracted from the numerical field computation for a general Drude dispersion model. $\tau = 0.2$ ps, $f = 40$ THz, $\rho = \lambda_0$.

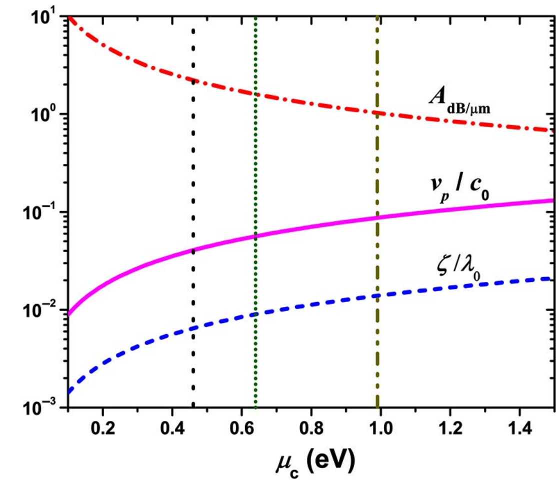

Fig. 8. Normalized phase velocity v_p/c_0, field confinement factor ζ/λ_0, and power attenuation $A_{\mathrm{dB}/\mu\mathrm{m}}$ versus μ_c for Drude (intraband) graphene model with $\tau = 0.35$ ps and $f = 40$ THz. The dot, short dot, and dash-dot-dot vertical lines represent the optimal μ_c from (16) and (17) for $\rho = 0.5\lambda_0$, $\rho = \lambda_0$, and $\rho = 2\lambda_0$, respectively.

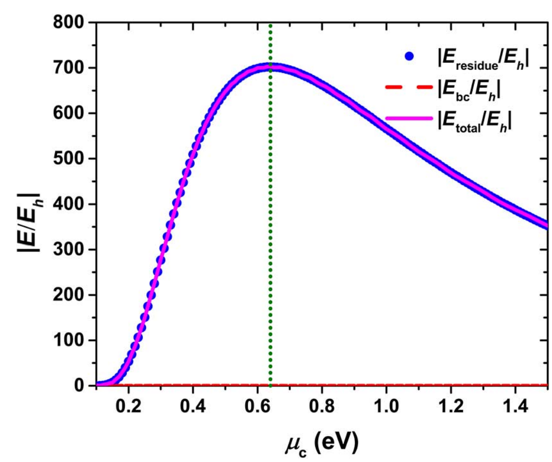

Fig. 9. Normalized electric fields versus μ_c for Drude (intraband) graphene model. The vertical line represents the optimal μ_c from the optimal σ_0 by (16) and (17). $\tau = 0.35$ ps, $f = 40$ THz, $\rho = \lambda_0$.

thin film having different thicknesses, along with the maximum normalized residue field for each thickness when changing σ_0. In order to extract the optimal σ_0 for each thickness from numerical results, we computed the field values varying σ_0 then found the maximum amplitude of field and recorded the corresponding σ_0 as the optimal σ_0. One can see that the simple formula (16) accurately predicts the optimal conductivity in the Drude model.

As a final example, we now consider one of the best-known examples of a 2-D material, the Drude model of graphene [12]. A graphene sheet can be considered as a two-sided impedance surface, and in the intraband approximation the surface conductivity is [11], [12]

$$\sigma_0^{\mathrm{intra}} = \frac{e^2 k_B T \tau}{\pi \hbar^2} \left[\frac{\mu_c}{k_B T} + 2 \ln \left(e^{\frac{-\mu_c}{k_B T}} + 1 \right) \right] \tag{17}$$

where $\hbar = h/2\pi$ is the reduced Planck's constant, k_B is the Boltzmann's constant, T is the temperature, and μ_c is the chemical potential. At sufficiently low frequencies, or for heavily-doped/strongly biased surfaces, graphene is well-modeled by the Drude conductivity. The conductivity of graphene can be adjusted by changing the chemical potential, and the problem of determining the optimal σ_0 can be cast in terms of finding the optimal value of μ_c. We assume room temperature $T = 300$ K and a relaxation time of graphene $\tau = 0.35$ ps [29].

Fig. 8 shows the normalized phase velocity, confinement factor, and power attenuation of the surface plasmon along the propagation (ρ) direction as a function of μ_c. Also shown is the optimal value of μ_c arising from $\sigma_{0,\mathrm{opt}}$ from (16) for several different positions. As expected, for larger values of ρ the optimal value of chemical potential results in lower attenuation. Fig. 9 shows the corresponding electric field. For very low values of chemical potential, the residue and branch cut fields are negligible, and the total field E_{total} reduces to the direct source-excited field E_h.

Fig. 10 shows a comparison between the optimal μ_c predicted by the simple formula (16) and the value determined (extracted) by numerically computing the field, along with the maximum normalized residue field for each frequency when

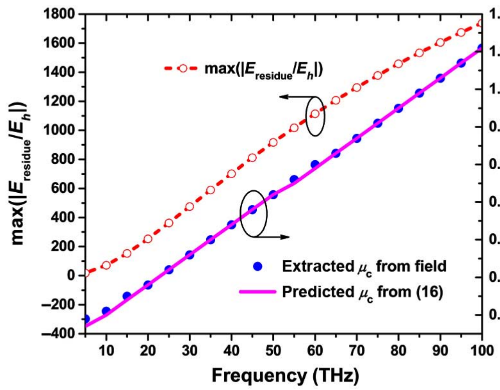

Fig. 10. Maximum normalized electric fields, predicted, and extracted optimal μ_c at different frequencies for Drude (intraband) graphene model $\rho = \lambda_0$.

changing μ_c. One can see that the predicted optimal values agree well with the full numerical results.

C. *Effects Beyond the Drude Model: Interband Transitions*

The Drude model is sufficient in many situations of interest, although at sufficiently high frequencies interband transitions can play an important role in the optical response of materials. For example, for graphene at frequencies where $\hbar\omega > 2\mu_c$, the full graphene conductivity is

$$\sigma = \sigma_{\text{intra}} - \frac{je^2}{\pi\hbar^2}(\omega - j\Gamma)\int_0^\infty \frac{f_d(-\xi) - f_d(\xi)}{(\omega - j\Gamma)^2 - 4(\xi/\hbar)^2}d\xi \tag{18}$$

where $\Gamma = 1/\tau'$ is the interband scattering rate ($\tau' = 0.0658$ ps is assumed in this work), ξ is energy, and $f_d(\xi) = \left[e^{(\xi-\mu_c)/(k_BT)} + 1\right]^{-1}$ is the Fermi–Dirac distribution. The second term of (18) is due to interband contributions. Importantly, $\sigma''_{\text{intra}} > 0$, yielding an inductive surface, whereas $\sigma''_{\text{inter}} < 0$, resulting in a capacitive surface. For metals, often interband effects are incorporated using measured data [30], or curve-fitted models [25]. In the following, we briefly consider the effect of interband transitions on optimum SP excitation.

Fig. 11 shows comparison of the maximum normalized electric fields and optimal μ_c for the Drude graphene model (only intraband) and the full graphene model (with the addition of the interband conductivity). The effect of the interband conductivity is negligible at frequencies of several THzs but more pronounced at higher frequencies, as expected. The inclusion of the interband contribution decreases the maximum electric field amplitude in high frequencies, and larger μ_c is needed to generate this SP field.

As another example, we consider a thin gold sheet whose surface conductivity is $\sigma = \sigma_{3\text{-D}}t$. When the thickness of metal films is near of below the electron mean free path (typically, about 40–50 nm at room temperature), various effects such as the presence of impurities, grain-boundary scattering, and surface scattering contribute to decreasing the conductivity of a metal film compared to a bulk sample, i.e., $\sigma_{3\text{-D}} = \sigma_{3\text{-D}}(t)$ [31]–[34]. A typical effect is to reduce the conductivity by a factor of 2–10, with the reduction factor depending on various

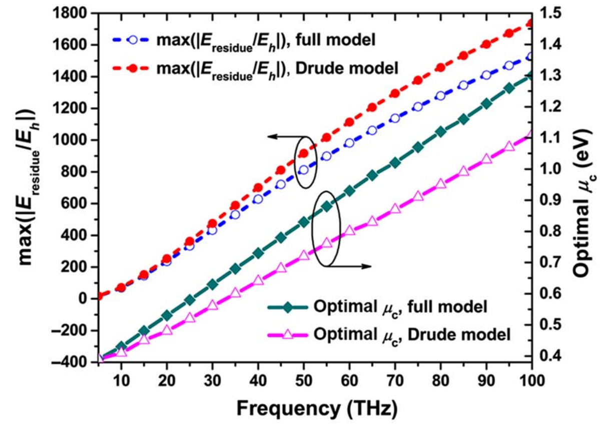

Fig. 11. Comparison of the maximum normalized electric fields and optimal μ_c for graphene considering the Drude (intraband) model and the more complete (intraband plus interband) model.

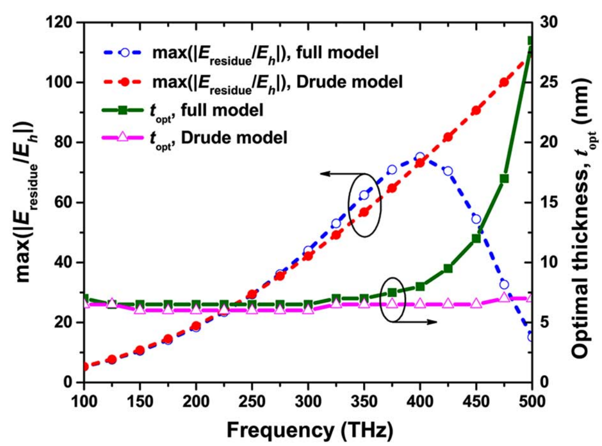

Fig. 12. Comparison of the maximum normalized electric fields and optimal thickness for gold sheet considering the Drude (intraband) model and the more complete (intraband plus interband) model.

parameters associated with the different scattering mechanisms. Here, for simplicity, we use a constant scaling factor α multiplying the bulk conductivity, i.e., $\sigma_{3\text{-D}}^{\text{film}} = \alpha\sigma_{3\text{-D}}^{\text{bulk}}$, with a value $\alpha = 0.2$.

For gold including interband effects, we use $\sigma_{3\text{-D}} = \alpha j\omega\varepsilon_0[\varepsilon_{\text{Au}}(\omega) - 1]$, where $\varepsilon_{\text{Au}}(\omega)$ can be calculated from the curve-fit formulas in [25]. Fig. 12 shows the maximum SP field and optimal thickness at different frequencies, calculated from the full model (including interband transitions) and from the Drude model. One can see that interband transitions are not important in the low frequency range between 100 and 400 THz, but have strong effects at higher frequencies, as expected.

D. *Effect of Spatial Dispersion*

Since we consider maximizing the SP field, it is important to consider the possible role that spatial dispersion may play since the surface plasmon may be quite slow [35]. Defining $\text{Re}(k_\rho^{SP})/k_0 = c_0/v_p = a$, it is shown in [35] that spatial dispersion may be important when $a > 100$ but less important if $a < 100$. From Fig. 8, we can see that the normalized phase

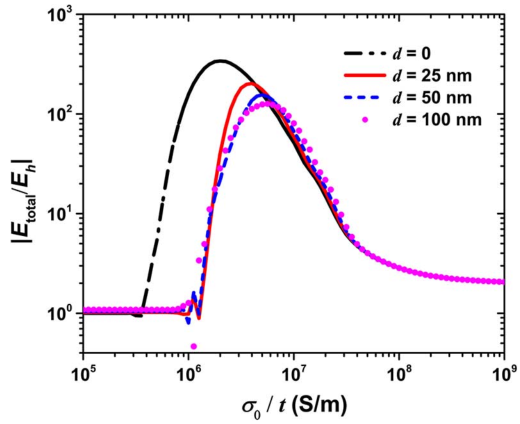

Fig. 13. Normalized electric fields versus σ_0/t for different substrate thicknesses, d. $f = 40$˜THz, $\tau = 0.2$ ps, $t = 10$ nm, $\rho = \lambda_0$.

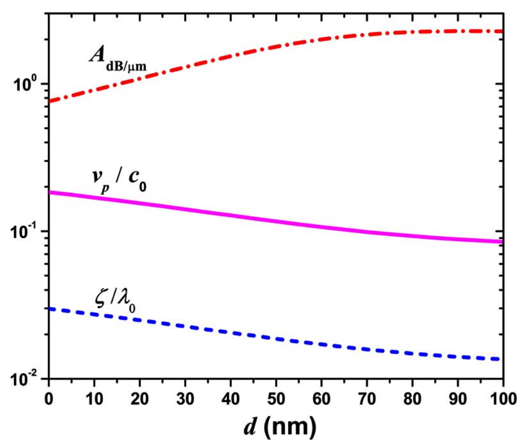

Fig. 14. Normalized phase velocity v_p/c_0, field confinement factor ζ/λ_0, and power attenuation $A_{\mathrm{dB}/\mu m}$ versus d for substrate-supported Drude conductive sheet. $f = 40$ THz, $\sigma_0/t = 5 \times 10^6$ S/m, $\tau = 0.2$ ps, $t = 10$ nm, $\rho = \lambda_0$.

velocity v_p/c_0 is larger than 0.01 at the optimal chemical potentials where the strongest SP wave can be obtained, i.e., $a < 100$ is satisfied. Therefore, the spatial dispersion does not have a significant effect on the obtained results in this work.

We validated this by direct calculation. Inclusion of spatial dispersion leads to an anisotropic conductivity tensor $\sigma_{\alpha,\beta}$, $\alpha, \beta = x, z$. For this case, we calculated the fields using the spatially dispersive conductivity tensor developed in [36] and the Green's function for anisotropic graphene [35]. The results with and without spatial dispersion were virtually identical (results not shown), and so we conclude that spatial dispersion effects are not important in the results here.

E. Effect of a Substrate

Although 2-D materials can be suspended across gaps in materials [37], often a substrate support is needed for practical applications. Here, the effects of a substrate on SP propagation characteristics are investigated. Referring to Fig. 1, we assume the substrate is SiO_2 with a thickness of d, and $\varepsilon_1 = \varepsilon_3 = \varepsilon_0$, $\varepsilon_2 = 4\varepsilon_0$. The conductive sheet is assumed to be a general Drude dispersive material with thickness of $t = 10$ nm and relaxation time $\tau = 0.2$ ps. Figs. 13 and 14 show the effects of a finite substrate on SP excitation and propagation. Increasing the thickness of the substrate will decrease the maximal field amplitude (at a given frequency), and a larger dc conductivity will be needed to obtain the field maximum. This tendency saturates for sufficiently-thick substrates (here, above approximately 100 nm) due to the confinement of the SP field. Fig. 14 shows that for a fixed dc conductivity σ_0, increasing the thickness of the substrate will lead to larger power attenuation (due to increasing field confinement, with a commensurate decrease in SP phase velocity).

V. Conclusion

The optimal surface conductivity for strong surface plasmon excitation and propagation on 2-D materials and thin films has been considered. We have shown that an optimum surface conductivity exists to maximize the SP field at a given position, and discussed the inherent tradeoff between propagation loss and near-field excitation amplitude/LDOS. Several general materials models (dispersionless, Drude dispersion, and interband transition) have been considered, and simple formulas were presented to obtain a maximal SP field at a given distance from a canonical source. Graphene and thin metal film examples were provided.

Appendix
Optimal Surface Characteristics-Based Solely on Modal SP Wavenumber

The main text describes optimization of the surface conductivity based on maximizing the SP electric field. Here, we present a different analysis based only on the modal wavenumber, exhibiting the tradeoff between modal field confinement and loss. For simplicity, we consider the dispersionless case.

Given (11) and (12), we can now consider the first three criteria for desirable SP characteristics based on the modal wavenumber. To satisfy the first two criteria (slow, nonradiative mode with tight energy confinement), we need $\sigma''/\varepsilon_r' \ll 1$. However, to have low propagation loss, from (11) we need σ''/ε_r'' large.[2]

Considering the competing interests of criteria 1–3, one method of determining an optimal surface is to set the maximum tolerable loss of the mode and find the smallest value of σ'' that does not violate the loss criterion. This will result in the mode with the best possible slow-wave factor and mode confinement for a given level of loss.

[2] As an aside, it is interesting to note that for a lossless surrounding medium ($\varepsilon_r'' = 0$) then the smaller σ'' becomes the slower the mode and the better the energy confinement to the surface. Maintaining $\sigma' \ll \sigma''$, as the material vanishes ($\sigma'' \to 0$), the mode becomes infinity slow and confined. However, in this case, one needs to be infinitesimally close to the surface to measure anything. More practically, there will always be some material loss in the dielectric (also generally $\sigma' \neq 0$). For a fixed $\varepsilon_r'' \ll \varepsilon_r'$, as σ'' becomes small, the loss becomes very large

$$\mathrm{Im}\,(k_\rho/k_0) \approx \frac{2}{\sigma''\eta_0}\left(\varepsilon_r'' + \frac{\varepsilon_r'\sigma'}{\sigma''}\right) \tag{19}$$

and so, were it even possible, the limit $\sigma'' \to 0$ is undesirable from a loss perspective.

For radial propagation along the surface and assuming $k_\rho \rho \gg 1$, $H_0^{(2)}(k_\rho \rho) \approx \sqrt{\frac{2}{\pi k_\rho \rho}} e^{-j\left(k_\rho \rho - \frac{\pi}{4}\right)}$, and loss is associated with $e^{-jk_\rho \rho} \propto e^{-\mathrm{Im}(k_\rho)\rho}$, and $A_{\mathrm{dB/m}} = 8.686 \mathrm{Im}\,(k_\rho)$ is attenuation in dB/m. Assuming that a value of D_0 dB/m is tolerable, then $\mathrm{Im}\,(k_\rho) \leq D_0/8.686$ such that

$$\sigma''_{\mathrm{opt}_1} \geq \frac{0.29\varepsilon''}{2D_0\lambda_0} + \frac{1}{2}\sqrt{\left(\frac{0.29\varepsilon''}{D_0\lambda_0}\right)^2 + 4\frac{0.29}{D_0\lambda_0}\varepsilon'_r\sigma'} \qquad (20)$$

as the optimal value of σ'' for a given level of tolerable loss (i.e., resulting in the tightest field confinement and largest slow-wave factor for a given loss value D_0).

Comparing (20) and (14), we see that (20) requires specification of a maximum tolerable attenuation (D_0), and results in a surface having the largest slow-wave factor and tightest field confinement for a given level of attenuation, whereas (14) requires specification of the observation position (ρ) and results in a surface that maximizes the SP electric field at the given point. The two expressions (20) and (14) are internally consistent for a given loss value. For example, for $\rho = \lambda_0$, $y = \lambda_0/100$, $\varepsilon'_r = 1$, $\varepsilon''_r = 0.001$, and $\sigma' = 10^{-6}$, at $f = 10$ THz, $\sigma''_{\mathrm{opt}} = 0.00025$, leading to $D_0 \approx 0.19\ \mathrm{dB}/\mu\mathrm{m}$ from (19) and $\zeta/\lambda_0 \approx 0.0076$ from (12). Setting $D_0 = 0.19\ \mathrm{dB}/\mu\mathrm{m}$, $\sigma''_{\mathrm{opt}_1} = 0.00025 = \sigma''_{\mathrm{opt}}$.

References

[1] J. Zhang, L. Zhang, and W. Xu, "Surface plasmon polaritons: Physics and applications," *J. Phys. D, Appl. Phys.*, vol. 45, no. 11, p. 113001, 2012.

[2] A. V. Zayats and I. I. Smolyaninov, "Near-field photonics: Surface plasmon polaritons and localized surface plasmons," *J. Opt. A, Pure Appl. Opt.*, vol. 5, no. 4, pp. S16–S50, 2003.

[3] W. Barnes, A. Dereux, and T. Ebbesen, "Surface plasmon subwavelength optics," *Nature*, vol. 424, pp. 824–830, 2003.

[4] J. Homola, S. Yeea, and G. Gauglitzb, "Surface plasmon resonance sensors: Review," *Sens. Actuators B Chem.*, vol. 54, pp. 3–15, 1999.

[5] B. Simkhovich and G. Bartal, "Plasmon-enhanced four-wave mixing for superresolution applications," *Phys. Rev. Lett.*, vol. 112, no. 5, p. 056802, Feb. 2014.

[6] C. Forestiere *et al.*, "Genetically engineered plasmonic nanoarrays," *Nano Lett.*, vol. 12, no. 4, pp. 2037–2044, 2012.

[7] W. Lu *et al.*, "Targeted photothermal ablation of murine melanomas with melanocyte-stimulating hormone analog–conjugated hollow gold nanospheres," *Clin. Cancer Res.*, vol. 15, pp. 876–886, 2009.

[8] E. Dreaden, A. Alkilany, X. Huang, C. Murphy, and M. El-Sayed, "The golden age: Gold nanoparticles for biomedicine," *Chem. Soc. Rev.*, vol. 41, pp. 2740–2779, 2012.

[9] S. A. Mikhailov and N. A. Savostianova, "Influence of contacts on the microwave response of a two-dimensional electron stripe," *Phys. Rev. B*, vol. 74, p. 045325, 2006.

[10] A. Mikhailov and K. Ziegler, "New electromagnetic mode in graphene," *Phys. Rev. Lett.*, vol. 99, p. 016803, 2007.

[11] G. Hanson, "Dyadic Green's functions and guided surface waves for a surface conductivity model of graphene," *J. Appl. Phys.*, vol. 103, no. 6, p. 064302, 2008.

[12] G. W. Hanson, A. B. Yakovlev, and A. Mafi, "Excitation of discrete and continuous spectrum for a surface conductivity model of graphene," *J. Appl. Phys.*, vol. 110, no. 11, p. 114305, 2011.

[13] A. Y. Nikitin, F. Guinea, F. J. Garcia-Vidal, and L. Martin-Moreno, "Fields radiated by a nanoemitter in a graphene sheet," *Phys. Rev. B*, vol. 84, no. 19, p. 195446, 2011.

[14] M. Jablan, M. Soljacic, and H. Buljan, "Plasmons in graphene: Fundamental properties and potential applications," *Proc. IEEE*, vol. 101, no. 7, pp. 1689–1704, Jul. 2013.

[15] A. Scholz, T. Stauber, and J. Schliemann, "Plasmons and screening in a monolayer of MoS2," *Phys. Rev. B*, vol. 88, pp. 035135, 2013.

[16] K. S. Novoselov *et al.*, "Electric field effect in atomically thin carbon films," *Science*, vol. 306, pp. 666–669, 2004.

[17] A. Manjavacas and F. G. de Abajo, "Tunable plasmons in atomically thin gold nanodisks," *Nat. Commun.*, vol. 5, p. 3548, 2014, doi: 10.1038/ncomms4548.

[18] C. L. Holloway *et al.*, "An overview of the theory and applications of metasurfaces: The two-dimensional equivalents of metamaterials," *IEEE Antennas Propag. Mag.*, vol. 54, pp. 10–35, Apr. 2012.

[19] M. A. Salem and C. Caloz, "Manipulating light at distance by a metasurface using momentum transformation," *Opt. Exp.*, vol. 22, pp. 14 530–14 543, 2014.

[20] A. V. Kildishev, A. Boltasseva, and V. M. Shalaev, "Planar photonics with metasurfaces," *Science*, vol. 339, pp. 1232009, 2013.

[21] G. Hanson, E. Forati, W. Linz, and A. Yakovlev, "Excitation of Thz surface plasmons on graphene surfaces by an elementary dipole and quantum emitter: Strong electrodynamic effect of dielectric support," *Phys. Rev. B*, vol. 86, pp. 235440, 2012.

[22] S. V. Gaponenko, *Introduction to Nanophotonics*. Cambridge, U.K.: Cambridge Univ. Press, 2010.

[23] A. Yaghjian, "Electric dyadic Greens functions in the source region," *Proc. IEEE*, vol. 68, pp. 248–263, Feb. 1980.

[24] L. Novotny and B. Hecht, *Principles of Nano-Optics*. Cambridge, U.K.: Cambridge Univ. Press, 2012.

[25] P. G. Etchegoin, E. Le Ru, and M. Meyer, "An analytic model for the optical properties of gold," *J. Chem. Phys.*, vol. 125, no. 16, p. 164705, 2006.

[26] F. S. Manciu *et al.*, "A Drude model analysis of conductivity and free carriers in boron-doped diamond films and investigations of their internal stress and strain," *J. Mater. Sci.*, vol. 49, no. 16, pp. 5782–5789, 2014.

[27] V. Geraldo, L. V. Scalvi, P. Lisboa-Filho, and C. Morilla-Santos, "Drude's model calculation rule on electrical transport in Sb-doped SnO2 thin films, deposited via sol–gel," *J. Phys. Chem. Solids*, vol. 67, no. 7, pp. 1410–1415, 2006.

[28] Z. Qiao, C. Agashe, and D. Mergel, "Dielectric modeling of transmittance spectra of thin ZnO: Al films," *Thin Solid Films*, vol. 496, no. 2, pp. 520–525, 2006.

[29] C. Lee *et al.*, "Optical response of large scale single layer graphene," *Appl. Phys. Lett.*, vol. 98, no. 7, p. 071905, 2011.

[30] P. B. Johnson and R.-W. Christy, "Optical constants of the noble metals," *Phys. Rev. B*, vol. 6, no. 12, p. 4370, 1972.

[31] K. Fuchs, "The conductivity of thin metallic films according to the electron theory of metals," *Math. Proc. Cambridge Philos. Soc.*, vol. 34, no. 1, pp. 100–108, 1938.

[32] E. H. Sondheimer, "The mean free path of electrons in metals," *Adv. Phys.*, vol. 1, no. 1, pp. 1–42, 1952.

[33] A. Mayadas and M. Shatzkes, "Electrical-resistivity model for polycrystalline films: The case of arbitrary reflection at external surfaces," *Phys. Rev. B*, vol. 1, no. 4, p. 1382, 1970.

[34] S. Rossnagel and T. Kuan, "Alteration of Cu conductivity in the size effect regime," *J. Vac. Sci. Tech. B*, vol. 22, no. 1, pp. 240–247, 2004.

[35] G. Hanson, "Dyadic Green's functions for an anisotropic, non-local model of biased graphene," *IEEE Trans. Antennas Propag.*, vol. 56, no. 3, pp. 747–757, Mar. 2008.

[36] G. Lovat, G. W. Hanson, R. Araneo, and P. Burghignoli, "Semiclassical spatially dispersive intraband conductivity tensor and quantum capacitance of graphene," *Phys. Rev. B*, vol. 87, no. 11, p. 115429, 2013.

[37] J. C. Meyer *et al.*, "The structure of suspended graphene sheets," *Nature*, vol. 446, pp. 60–63, 2007.

Feng Liang was born in Hubei, China, in 1983. He received the B.S. degree in applied physics from the University of Electronic Science and Technology of China (UESTC), Chengdu, China, in 2006, and the Ph.D. degree in electrical engineering from Wuhan University, Wuhan, China, in 2011.

Since July 2011, he has been a Faculty Member with the School of Physical Electronics, UESTC, where he is now an Associate Professor. From April 2014 to March 2015, he was a Visiting Scholar with the Department of Electrical Engineering and Computer Science, University of Wisconsin–Milwaukee, Milwaukee, WI, USA. His research interests include theory, computation, and application of electromagnetic fields.

Alexander B. Yakovlev (S'94–M'97–SM'01) received the Ph.D. degree in radiophysics from the Institute of Radiophysics and Electronics, National Academy of Sciences, Kiev, Ukraine, in 1992, and the Ph.D. degree in electrical engineering from the University of Wisconsin–Milwaukee, Milwaukee, WI, USA, in 1997.

In 2000 (summer), he joined the Department of Electrical Engineering, University of Mississippi, Oxford, Mississippi, as an Assistant Professor and became an Associate Professor in 2004. Since July 2013, he has been a Full Professor of Electrical Engineering. He is a co-author of the book *Operator Theory for Electromagnetics: An Introduction* (Springer: New York, NY, USA, 2002). His research interests include mathematical methods in applied electromagnetics, homogenization theory, high-impedance surfaces for antenna applications, electromagnetic band-gap structures, metamaterial structures, wire media, graphene, cloaking, theory of leaky waves, transient fields in layered media, catastrophe, and bifurcation theories.

Dr. Yakovlev was an Associate Editor-in-Chief of the *ACES Journal* from 2003 to 2006 and an Associate Editor of the IEEE TRANSACTIONS ON MICROWAVE THEORY AND TECHNIQUES from 2005 to 2008. He is a member of URSI Commission B. He was the recipient of the Young Scientist Award at the 1992 URSI International Symposium on Electromagnetic Theory, Sydney, Australia, the Young Scientist Award at the 1996 International Symposium on Antennas and Propagation, Chiba, Japan, and a Junior Faculty Research Award at the School of Engineering, University of Mississippi in 2003.

George W. Hanson (S'85–M'91–SM'98–F'09) was born in Glen Ridge, NJ, USA, in 1963. He received the B.S. degree from Lehigh University, Bethlehem, PA, USA, the M.S. degree from Southern Methodist University, Dallas, TX, USA, and the Ph.D. degree from Michigan State University, East Lansing, MI, USA, all in electrical engineering, in 1986, 1988, and 1991, respectively.

From 1986 to 1988, he was a Development Engineer with the General Dynamics, Fort Worth, TX, USA, where he worked on radar simulators. From 1988 to 1991, he was a Research and Teaching Assistant with the Department of Electrical Engineering, Michigan State University. He is currently a Professor of Electrical Engineering and Computer Science with the University of Wisconsin–Milwaukee, Milwaukee, WI, USA. He is a co-author of the book *Operator Theory for Electromagnetics: An Introduction* (Springer: New York, NY, USA, 2002), and the author of *Fundamentals of Nanoelectronics* (Prentice-Hall: Englewood Cliffs, NJ, USA, 2007). His research interests include nanoelectromagnetics, quantum optics, mathematical methods in electromagnetics, and electromagnetic wave phenomena in layered media.

Dr. Hanson is a member of URSI Commission B, Sigma Xi, and Eta Kappa Nu, and was an Associate Editor for the IEEE TRANSACTIONS ON ANTENNAS AND PROPAGATION from 2002 to 2007. In 2006, he was the recipient of the S.A. Schelkunoff Best Paper Award from the IEEE Antennas and Propagation Society.